

## Subproject C3.3

# Computation of Electronic and Intermolecular Interactions

**Principal Investigator: Wim Klopper**

**CFN-Financed Scientists: to be inserted by the CFN administration**

**Further Scientists: Florian A. Bischoff, Heike Fliegl, Sebastian Höfener, Andreas Mavrandonakis, Tobias Pankewitz, David P. Tew**

**Abteilung für Theoretische Chemie, Institut für Physikalische Chemie  
Karlsruher Institut für Technologie, KIT-Campus Süd**

**Abteilung für Theoretische Chemie, Institut für Nanotechnologie  
Karlsruher Institut für Technologie, KIT-Campus Nord**

## Computation of Electronic and Intermolecular Interactions

### Introduction and Summary

The computation of electronic and intermolecular interactions in molecule-based nanostructures is instrumental in understanding their properties (e.g., crystal structures, magnetic properties) and designing new functional nanostructures. Properties of isolated nanostructures change significantly through interactions with their surroundings (e.g., surface, matrix, solvent). Furthermore, hydrogen bonding often plays a crucial role in biological as well as crystal structures of inorganic clusters. The accurate and thus reliable *ab initio* calculation of these interactions is an important but challenging task for molecular systems on the nanoscale. Today, density-functional theory (DFT) provides the only *ab initio* computational method that can be applied in a general and routine manner to large systems (with hundreds of atoms), but this theory has serious deficiencies in particular in the calculation of weak long-range intermolecular interactions and (anti) ferromagnetic couplings in transition-metal complexes. This means that DFT calculations must be carried out along with empirical corrections and/or with validation/benchmark studies with highly correlated wave functions, assuming that these have been calibrated against experimental data.

Below, a number of examples of DFT calculations that were performed during the last CFN funding period will be presented. Most of these calculations had been motivated by work of, or were carried out in close collaboration with, experimental groups in the CFN. The calculations include investigations of the nature of the interactions between fullerene molecules. They had been motivated by experiments on thin films of various fullerenes that had been exposed to atomic hydrogen. It turned out that intercage fullerene···fullerene binding occurs for non-IPR fullerenes such as C<sub>58</sub> and a non-IPR isomer of C<sub>60</sub>, whereas the normal IPR fullerene C<sub>60</sub> only shows weak van der Waals interactions. (IPR fullerenes are those that obey the isolated pentagon rule.) The fullerene studies are presented in Section 1. They contain DFT calculations with empirical (dispersion) corrections as well as benchmark calculations with highly correlated wave functions.

Further examples of DFT calculations that are benchmarked against highly correlated wave functions are provided by the calculations of magnetic exchange couplings in Section 2. At the DFT level, the Noodleman approach with symmetry-broken determinants was applied, and the corresponding results were compared to results obtained at the multi-reference configuration interaction level. Furthermore, magnetic susceptibilities were computed and compared to experimental data obtained in experimentally oriented subprojects of the CFN. The calculations confirmed the known strong dependence of broken-symmetry DFT calculations on the functional used, whereas an excellent agreement with experiment was achieved by a *modified* configuration interaction (MCI) approach that had been designed specifically for the purpose of computing magnetic exchange couplings.

Intermolecular interactions between small molecules and single-walled carbon nanotubes are reported in Section 3. A dispersion-corrected DFT approach (denoted DFT-D) was used after benchmarking it against high-level calculations. Section 4 provides several further examples of intermolecular interactions such as hydrogen bonding and  $\pi$ - $\pi$  stacking interactions between aromatic ring systems. Chains or H-bonded water molecules and H-bonded 3D frameworks inside inorganic cluster compounds have also been studied. Interactions with solvents are studied at several places. Furthermore, unusual chemical bonds between Al, Si and Ge were investigated and results are reported in Section 5. While these bonds cannot be characterized as weak intermolecular interactions, they are very interesting from the viewpoint of the chemistry of diradicals, or rather

diradicaloids, as the bonding turned out to be (to some extent) diradical in nature. Also in this case, DFT calculations on the large inorganic clusters were accompanied by high-level (multi-reference) wave function calculations on small but representative model systems.

Finally, in Section 6, efforts in method development are reported. Wave-function-based methods have been developed further using expansions in terms of Slater-type geminals. Efficient codes have been written for use of these geminals at the second-order Møller–Plesset (MP2) level, including scalar and spin–orbit relativistic corrections. Moreover, the implementation of Slater-type geminals at the coupled-cluster level has been completed, and calculations with unprecedented accuracy have been performed on small systems.

### 1. Interactions and Reactivity of Fullerenes: Hydrogenation and Intercage Binding

The main focus of the subproject's research in this field is on the computational investigation of new carbon materials composed of non-IPR fullerene cages. The aim is to support and explain experimental data and to make predictions concerning the stability and properties of not yet synthesized molecules. An efficient approach that allows the systematic investigation of fullerene derivatives of the type  $C_nH_{2x}$  has been developed and tested [C3.3:35]. The procedure yields a set of low-energy structures for each investigated composition that can be used to construct energetically favored reaction pathways. It thus enables the prediction of particularly stable structures by means of analysis of the respective reaction energies. Furthermore, the low energy structures of  $C_nH_2$  give information about the most reactive sites in the fullerene cage  $C_n$ . Based on these  $C_nH_2$  structures, the presumably best candidates for dimers formed via [2+2] cycloaddition reactions can be derived. In the following, results are presented for both the determination of particularly stable fullerene hydride structures and the construction of [2+2] dimers based on  $C_nH_2$  structures. Both projects were motivated by experimental findings and were partially carried out in close collaboration with the group of Kappes (subproject C4.6).

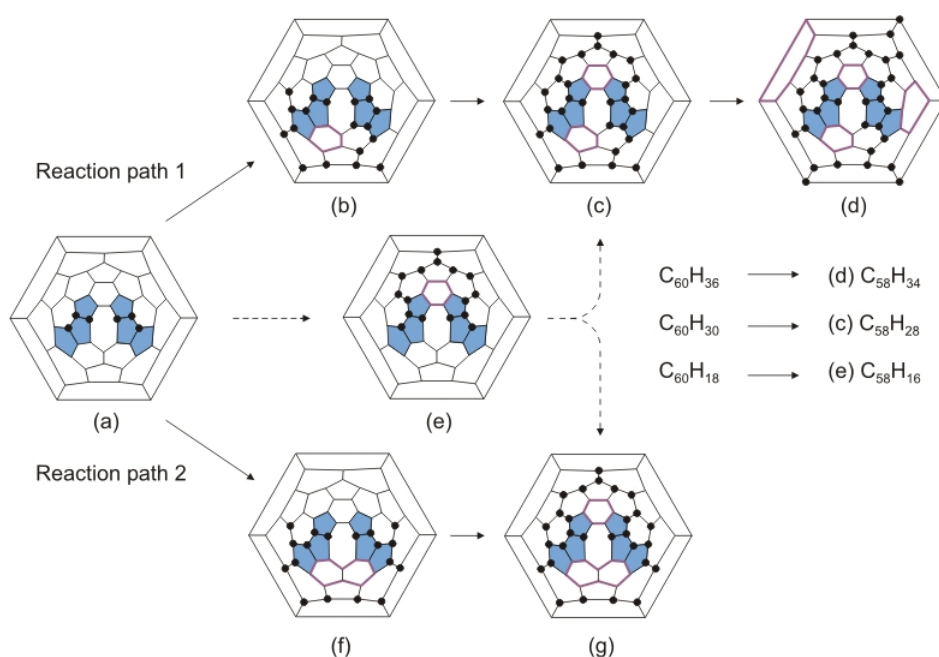


Figure 1: Schlegel diagrams for the theoretically predicted particularly stable hydride structures  $C_{58}H_6$  (a),  $C_{58}H_{18}$  (b,f),  $C_{58}H_{28}$  (c,g) and  $C_{58}H_{34}$  (d).

The hydrogenation of  $C_{58}$  was studied in order to predict the preferably formed products [C3.3:41]. Several particularly stable structures were identified and corresponding stability criteria were established, such as saturation of the most reactive sites and formation of aromatic domains (Figure 1). Moreover, a structural connection between stable  $C_{58}$  and  $C_{60}$  hydrides was found.

$C_{60}$  films produced from gas phase  $C_{60}^+$  obtained by fragmentation of  $C_{70}$  show significantly different properties than films composed from well-known  $C_{60}-I_h$ . It was suggested that a new material consisting of non-IPR  $C_{60}$  isomers was created [C3.3:43]. Therefore, the energetically lowest non-IPR isomer of  $C_{60}$ ,  $C_{60}-C_{2v}$ , was studied with respect to the formation of dimers and higher aggregates. The structures of the examined dimers were constructed based on the energetically most stable  $C_{60}H_2$  isomers that allow for [2+2] cycloaddition by replacing the C-H bonds with intercage bonds (Figure 2).

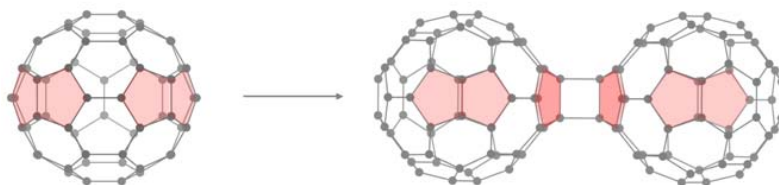


Figure 2: [2+2] cycloaddition of non-IPR  $C_{60}$  yielding a dimer that is linked via the carbon atoms of fused pentagonal rings (highlighted in red).

For comparison with experimental thermal desorption and photoelectron spectra, dimer binding energies were computed and photoelectron spectra of the various species ( $C_{60}-I_h$ ,  $C_{60}-C_{2v}$ , and corresponding dimers) were simulated. The results revealed that the high thermal stability as well as the electronic properties of the new material can only be explained via linked non-IPR  $C_{60}$  cages (Figure 3).

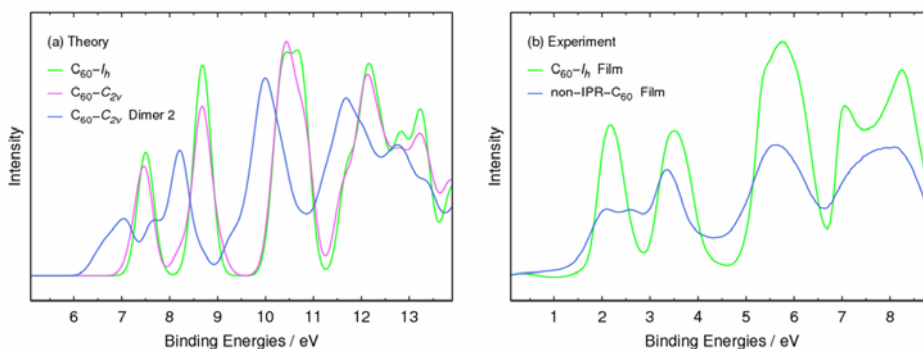


Figure 3: Comparison of simulated photoelectron spectra for various species (a) and measured photoelectron spectra of  $C_{60}-I_h$  films and the new material (b). The shift to lower energies and the additional band can only be reproduced with intercage binding.

## 2. Magnetic Interactions: Exchange Coupling and Ring Currents

Transition-metal compounds are promising materials for magneto-optical devices or storage materials. Thus, the investigation of their magnetic properties is of technical interest. Quantum

chemical calculations were performed in order to obtain a detailed understanding of magnetic properties of transition-metal compounds. In particular, the magnetic exchange coupling in polynuclear systems was investigated. The computational studies were motivated by experimental findings of, and partially carried out in close collaboration with, the group of Powell (subproject C1.2).

In Ref. [C3.3:17], different quantum chemical approaches to obtain the magnetic exchange coupling constants were compared mutually as well as with experimental data. Magnetic susceptibility measurements on the compound  $[\text{Fe}_2(\text{hpdt})_2(\text{H}_2\text{O})_3\text{Cl}]$  showed that the Fe-centers have a Fe(III) high-spin conformation, and a magnetic exchange coupling constant of  $-14.5 \text{ cm}^{-1}$  was obtained. The results of density functional calculations were strongly dependent on the functional used. The calculated coupling constants varied by more than a factor of two. In an attempt to study to what extent it is possible to undertake configuration-interaction calculations on such binuclear compounds, multi-reference configuration-interaction (MRCI) calculations were performed on a  $[\text{Fe}_2(\text{OH})_5(\text{H}_2\text{O})_3(\text{NH}_3)_2\text{Cl}]$  model complex. The results showed that, when correlating only the ten iron 3d orbitals and the four valence orbitals of the bridging OH group, the calculated splitting is still by a factor of about four smaller than the value for the splitting inferred from magnetic susceptibility measurements. Modified valence configuration interaction (MCI) calculations were performed to approximately take into account the influence of orbital relaxation effects of all occupied orbitals in the excited configurations. The exchange splitting was significantly increased, but was still smaller than the experimental value.

The magnetic exchange coupling in polynuclear compounds was investigated in a tetranuclear Mn complex that serves as a model compound for photosystem II [C3.3:44]. The compound is a mixed valence compound with three Mn(III) centers and one Mn(II) center.

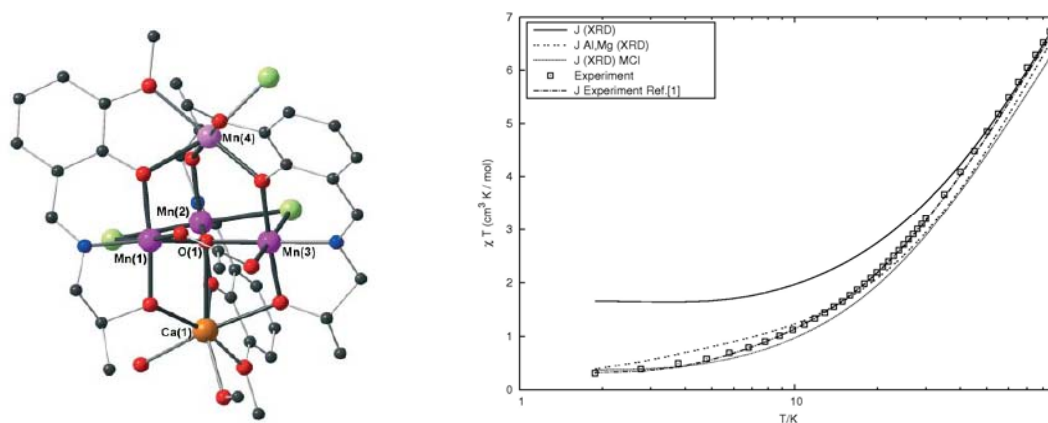


Figure 4: Structure and magnetic susceptibilities of the tetranuclear Mn complex. Color code: black (C), grey (H), pink (Mn), yellow (Ca), green (Cl), blue (N), red (O).

All six possible coupling constants were calculated by *ab initio* methods in order to obtain a detailed understanding of the magnetic behavior of the system. Again, the broken-symmetry approach of Noodleman was applied using density functional theory (B3LYP functional). Two different approaches were compared. On the one hand, the coupling constants were obtained from calculations on eight different determinants that describe the high-spin state as well as different broken-symmetry states of the tetranuclear cluster (method 1). On the other hand, a pair approach that permits a direct calculation of the individual coupling constants was used (method 2). For the pair approach, the coupling constants were also obtained from modified CASCI (complete active space configuration interaction) calculations (method 3). With the different sets of coupling

constants, the full Heisenberg Hamiltonian of the tetranuclear problem was used to calculate the magnetic susceptibilities, which were then compared with the corresponding experimental values. The susceptibility obtained with method 1 (J(XRD) in Figure 4) showed the wrong behavior at low temperatures, because the calculated ground state had the wrong spin multiplicity ( $S=3/2$  instead of  $S=1/2$ ). The results obtained with the pair approach revealed better agreement with experiment than method 1, but the modified CASCI calculations (J (XRD) MCI in Figure 4) outperformed the DFT calculations (J Al,Mg (XRD) in Figure 4).

Furthermore, the magnetic coupling in the compound  $[\text{Cu}_{30}\text{Fe}_2\text{Se}_6(\text{SePh})_{24}(\text{dppm})_4]$  (Figure 5) was investigated [C3.3:50]. The formal oxidation states of the iron atoms were determined experimentally by Mössbauer spectroscopy to be +3, in agreement with the quantum chemical calculations and the modeling of the magnetic data. Being able to estimate the coupling constant from quantum chemical calculations was crucial for extracting a value for  $J$  from the experimental data.

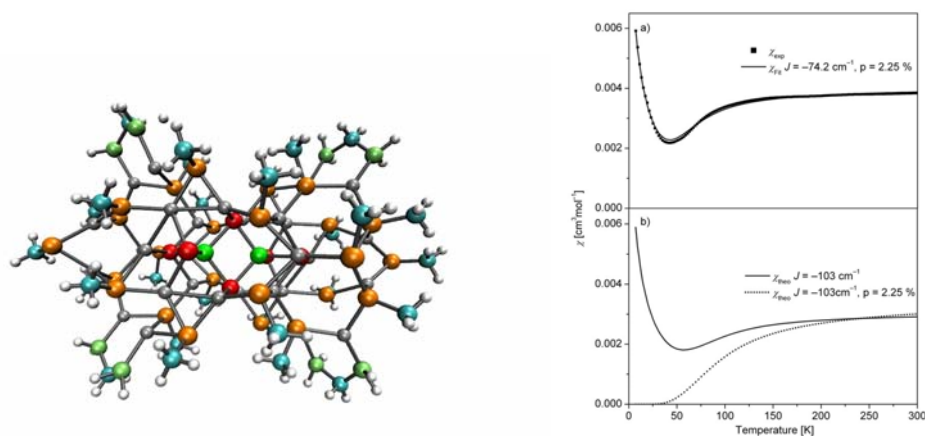


Figure 5: Structure (left) and magnetic susceptibility (right) of  $[\text{Cu}_{30}\text{Fe}_2\text{Se}_6(\text{SePh})_{24}(\text{dppm})_4]$ . Color code: green (Fe), red and orange (Se), grey (Cu), blue (C), green metallic (P), white (H).

Magnetically induced ring currents were studied both in (hypothetical) hydrocarbon nanorings as well as in small, representative aromatic, anti-aromatic, homo-aromatic, and non-aromatic ring-shaped hydrocarbons [C3.3:39, C3.3:46]. The current densities for these hydrocarbons were studied at the DFT and MP2 levels using gauge-including atomic orbitals, that is, by using the gauge-including magnetically induced current (GIMIC) approach. The calculations showed that all studied hydrocarbon rings sustain strong diatropic and paratropic ring currents when exposed to an external magnetic field, regardless whether they are unsaturated or not. Part of this work was performed with the aim to provide reference data for studies of dynamic response of molecular nanostructures in subproject C3.11.

### 3. Interactions with Single-Walled Carbon Nanotubes

The weak interaction of the primary alcohol molecules methanol (MeOH) and ethanol (EtOH) with the outer (exohedral binding) and inner (endohedral binding) sides of various armchair single-walled carbon nanotubes (SWCNTs; with diameters from 0.53 to 1.62 nm) were investigated by means of DFT calculations including an empirical energy correction for dispersion (DFT-D).

In a first exploratory computational study of the MeOH $\cdots$ SWCNT interaction [C3.3:23], the accuracy of the relatively new DFT-D approach was demonstrated by benchmarking it to high-level wave function calculations on small model systems. In a second, more recent study [C3.3:57], both alcohols MeOH and EtOH were investigated in more detail using the calibrated method and best empirical parameters. It was found that endohedral adsorption sites are favored over the exohedral ones (Figure 6).

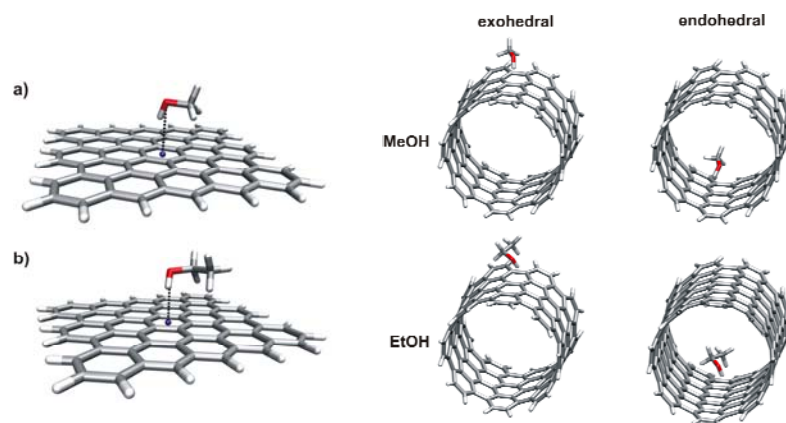


Figure 6: Left: Alcohol molecules interacting with a layer of graphene, modeling an infinite-diameter tube (zero-curvature); a) interaction of MeOH; b) interaction of EtOH. Right: Interaction of the primary alcohols MeOH and EtOH with the outer (exohedral) and the inner (endohedral) surface of the finite armchair (8,8) SWCNTs. The diameter of the tubes is 1.08 nm.

#### 4. Weak Van-der-Waals Interactions

Quantum chemical calculations were performed on the co-metal-free asymmetric conjugate addition reaction of dialkylzinc reagents with aldehydes. The reaction is catalyzed by a [2,2]paracyclophane-imine-zinc-methyl complex (Figure 7) and shows a negative nonlinear effect in enantio-selectivity (NLE). The origin of the NLE is the existence of a monomer–dimer equilibrium of the catalytically active complex.

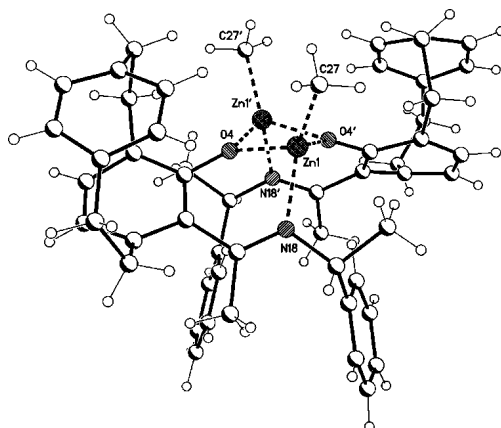


Figure 7: Molecular structure of the [2,2]paracyclophane-imine-zinc-methyl complex.

The stability of the monomers and different diastereomers of the dimers was studied by means of DFT calculations. Since the relative energies were strongly influenced by van der Waals inter-

actions, it was necessary to estimate (in the calculations) the complex stabilization by toluene solvent molecules [C3.3:58].

*Ab initio* DFT calculations were performed on complexes of various crown ethers with the dibenzylammonium cation. This computational work was motivated by experimental work performed in the Bräse group (subproject C5.2) towards the synthesis of functionalized organic nanostructures such as systems containing six [2]pseudorotaxanes, each built from a dibenzylammonium cation inside a crown ether, arranged octahedrally around a C<sub>60</sub> fullerene. Various crown ethers were investigated. Figure 8 shows the molecular electrostatic potential (MEP) and the equilibrium geometry of the dibenzylammonium complex with dibenzo-24-crown-8. The dibenzylammonium<sup>+</sup>crown ether [2]pseudorotaxanes are particularly interesting from a computational point of view, because they have much conformational freedom, and because they display competing intermolecular interactions such as N<sup>+</sup>-H<sup>+</sup>⋯O hydrogen bonds *versus* van der Waals-type  $\pi$ - $\pi$  stacking interactions. The large number of local minima on the conformational surface were addressed by using a genetic algorithm to search for the (global) lowest-energy structure at the DFT level. The structures found at this level were checked by re-computing their energies at the level of MP2 theory. In other work, detailed studies had been performed on various hydrogen bonds (e.g., N-H<sup>+</sup>⋯ $\pi$ ) and  $\pi$ - $\pi$  stacking interactions, in particular concerning the performance of MP2 and spin-component-scaled MP2 calculations [C3.3:19, C3.3:21, C3.3:29, C3.3:42, C3.3:54, C3.3:60]. The geometries of the [2]pseudorotaxanes were optimized at the spin-component-scaled MP2 level in a large basis set of atomic orbitals (def2-TZVPP).

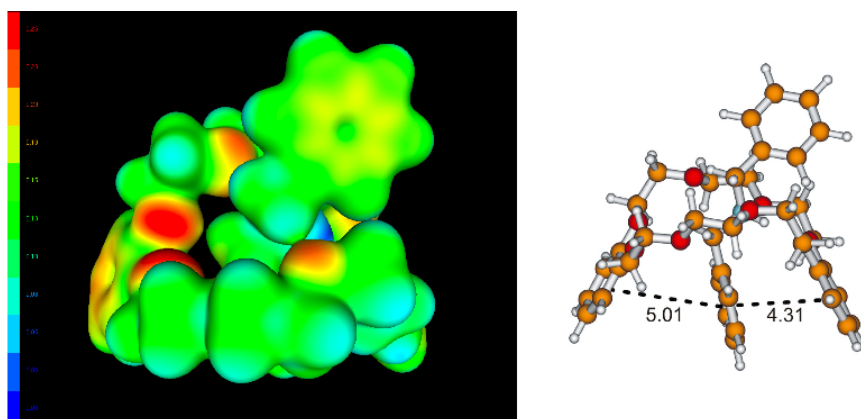


Figure 8: Left: MEP displayed on the 0.012 a.u. isodensity surface for the lowest-MP2-energy structure. The potential ranges from  $-0.01$  (dark blue) to  $-0.25$  a.u. (red). Right: ball-and-stick representation of the dibenzylammonium complex with dibenzo-24-crown-8 in the geometry with lowest MP2 single-point energy, indicating benzene-ring centroid-centroid distances in Å.

Further examples of calculations on hydrogen-bonded systems (e.g., water tapes) can be found in Refs. [C3.3:45] and [C3.3:48]. The weak van der Waals interactions between carbon dioxide and nitrogen-containing hydrocarbons were studied in Ref. [C3.3:40]. Other works [C3.3:37, C3.3:59] describe studies of [59]- and [60]fullerene cages with an orifice large enough for atoms and small molecules to pass through. A phosphate group that can easily be attached and removed from the edge of the orifice acted as a plug for the [60]fullerene vial, making it a nanoscale “water bottle.” With the plug attached (pictured right in Figure 9), a water molecule can leave the “bottle” only about 230 times slower than without it (pictured left in Figure 9). The experimental dynamic <sup>1</sup>H NMR measurements were accompanied by DFT calculations of the reaction barrier heights. Since

the experimental measurements were performed in solution, the computed gas-phase barriers were corrected for solvent effects employing a continuum-solvation model (COSMO: conductor-like screening model). The corrections were estimated by comparing the potential curves of a trajectory of the water molecule moving towards the orifice with and without the COSMO model. Whereas the barrier height for entering the cage was significantly increased (i.e., by 25 to 32 kJ mol<sup>-1</sup>), the barrier height for leaving the cage was hardly affected, owing to the fact that the main effect of the COSMO model was to stabilize the free water molecule, but not the water molecule inside the cage.

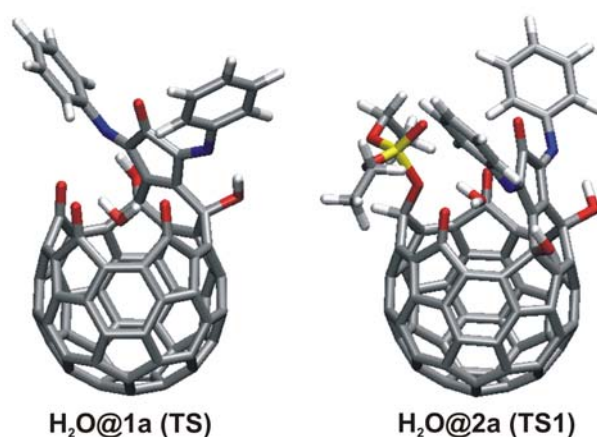


Figure 9: Transition-state (TS) structures for the water molecule leaving the cage of **1a** (fullerene cage without plug) and **2a** (cage with plug), respectively. The calculated barrier heights were computed to be 106 and 129 kJ mol<sup>-1</sup>, respectively.

## 5. Clusters: Novel Compounds of Main-Group Elements

Strictly speaking, are the systems described in this section not systems with (weak) intermolecular interactions. They possess, however, unusual single bonds ( $\sigma$  bonds) between main-group elements such as Al, Si, and Ge. In collaboration with the group of Schnöckel (subproject C1.3), Al–Al single bonds were studied.

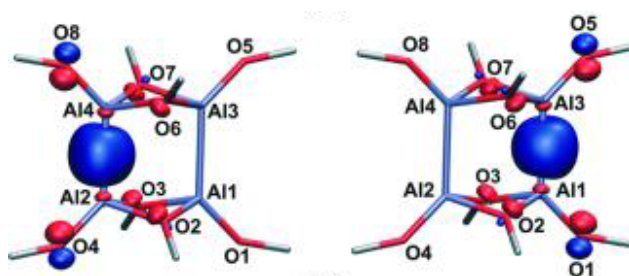


Figure 10: Localized frontier orbitals (highest occupied molecular orbitals) of the  $[\text{Al}_2(\text{O}t\text{Bu})_4]_2$  dimer, revealing two localized Al–Al  $\sigma$  bonds. For clarity, only the tertiary carbon atoms of the *t*Bu groups are shown (in silver), not the methyl groups.

As an example, the bonding situation in  $[\text{Al}_2(\text{O}t\text{Bu})_4]_2$  is considered, which can best be described by the formation of new bonds between the Al1/Al3 and Al2/Al4 atoms of different “butterfly” monomers [C3.3:38], thereby weakening the intramolecular Al1/Al2 and Al3/Al4 bonds. This is underlined by an analysis of the frontier orbitals (Figure 10), which have their main contributions between the Al1 and Al3 atoms (and between Al2 and Al4), but yield no significant electron density

between the Al1 and Al2 atoms (and Al3 and Al4). The monomer was extensively studied both experimentally and theoretically also with the ligand  $-PrBu$ , thereby considering various  $Al_2(PrBu_2)_4$  isomers. The “butterfly” structure of this compound has a direct Al–Al  $\sigma$  bond (appearing as bow-shaped orbital) of about 2.6 Å [C3.3:38, C3.3:47].

Unusual  $\sigma$  bonding also occurs between bridgehead atoms in propellanes. In particular, the pentasilapropellane pictured on the left of Figure 11 was investigated both at the DFT and at the complete-active-space self-consistent field (CASSCF) levels of theory [C3.3:56]. (The CASSCF calculations were performed on a  $Si_5$  model system.)

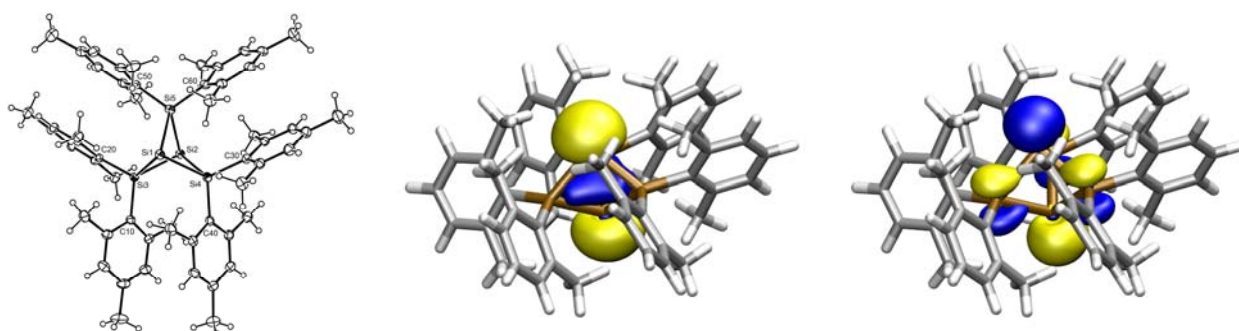


Figure 11: Experimental structure of the recently synthesized pentasilapropellane compound (left) together with the bonding (center) and anti-bonding (right) orbitals between the bridgehead Si atoms.

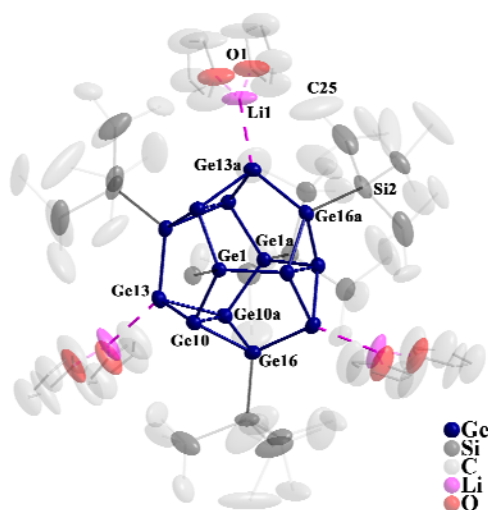


Figure 12: Molecular structure of  $Ge_{14}[Si(SiMe_3)_3]_5[Li(THF)_2]_3$  (without hydrogen atoms); vibrational ellipsoids with 50% probability.

The formation of a singlet hexaradicaloid metalloid  $Ge_{14}[Si(SiMe_3)_3]_5[Li(THF)_2]_3$  cluster from three singlet biradicaloid fragments was studied recently in collaboration with the groups of Schnepf and Schnöckel (subproject C1.3). In CASSCF calculations on a model of the  $Ge_{14}$  core, three bonding orbitals with occupation numbers significantly smaller than 2 were found, along with three corresponding anti-bonding orbitals with occupation numbers significantly larger than 0. This observation suggested a weakening of the three Ge10–Ge10a bonds (Figure 12), indicating a

radicaloid character. The bonding was found to be comparable to the weak bonding between the bridgehead atoms in pentasila- and pentagermapropellanes [C3.3:56].

The metalloid clusters may be viewed as model compounds for the area between molecules and the solid state, and thus, the observed multi-radicaloid character in the Ge<sub>14</sub> compound may be of importance for nanoparticles and surfaces where unsaturated Ge atoms are found. The multi-radicaloid character may be the reason for the differences in physical and chemical properties between nanoparticles and the bulk phase, for example, the reason for a strong size-dependent photoluminescence (PL) of germanium nanoparticles *versus* no comparable PL in elemental germanium.

## 6. Method Development

In Sections 1 to 5, a number of different *ab initio* quantum chemical methods have been applied to various problems of current interest, mostly in collaboration with other researchers of the CFN. These methods include DFT approaches (using different functionals and empirical corrections), second-order perturbation theory (also in the spin-component-scaled variant), coupled-cluster theory, all the way up to the multi-reference configuration-interaction methods. In subproject C3.3, second-order perturbation theory and coupled-cluster methods have been developed further by adding “explicitly correlated” functions—which depend on the interelectronic coordinates through Slater-type geminals (STGs)—to the conventional wave-function expansion in terms of Slater determinants, that is, in terms of orbital products (cf. Ref. [C3.3:16]).

Progress was made at the coupled-cluster level both in terms of computer implementations and in terms of new wave-function models. Computer codes have been developed in the framework of the DALTON (pioneering, exploratory implementation) and TURBOMOLE (efficient implementation) programs for applications of explicitly correlated coupled-cluster theory. In the framework of this theory, quintuple-zeta quality correlation energies could be computed in a triple-zeta basis only [C3.3:18]. Moreover, the development of a *diagonal* orbital-invariant form of the explicitly correlated coupled-cluster theory has turned out to be very useful for practical calculations [C3.3:26]. Explicitly correlated coupled-cluster theory has been applied at a few occasions during the last funding period, for instance in Refs. [C3.3:35], [C3.3:36], and [C3.3:51].

At the explicitly correlated second-order perturbation theory level, progress was made in terms of program efficiency (e.g., in terms of integral evaluation, code parallelization, novel models, open-shell approaches) [C3.3:30, C3.3:34] while the theory was also developed further to include scalar and spin-orbit relativistic effects using effective core potentials and a two-component quasi-relativistic treatment [C3.3:34, C3.3:52, C3.3:53]. Nuclear gradients were computed analytically in Ref. [C3.3:60] to optimize the equilibrium geometries of various hydrogen-bonded complexes.

All of the above mentioned developments will allow for more accurate, faster and larger second-order perturbation theory and coupled-cluster theory calculations with STGs in the future. They are valuable methods for the subproject C3.3 when highly accurate computational data are required or for the purpose of benchmarking and validating computationally less demanding methods.